




# Influence of Cu on the microstructure and corrosion resistance of cold-rolled type 204 stainless steels

Xiaohong Liu<sup>1</sup> · Lele Liu<sup>1</sup> · Fengli Sui<sup>2</sup> · Hongyun Bi<sup>3</sup> · E Chang<sup>3</sup> · Moucheng Li<sup>1</sup> 

Received: 30 January 2020 / Revised: 27 March 2020 / Accepted: 21 April 2020 / Published online: 4 May 2020  
© Springer-Verlag GmbH Germany, part of Springer Nature 2020

## Abstract

The microstructure and corrosion behavior in 3.5% NaCl solution of type 204 metastable austenitic stainless steels with 15% cold-rolling reduction and different Cu contents (i.e., 0, 0.87, and 1.46%) were investigated by X-ray (XRD), electron beam backscatter diffraction (EBSD), X-ray photoelectron spectroscopy (XPS), and electrochemical measurement techniques. Due to the suppressive effect of alloying Cu on the martensite transformation, both  $\alpha'$ - and  $\varepsilon$ -martensite phases show lower volume fractions in the specimens with higher Cu contents. The Cu addition results in forming the passive films with higher Cr/Fe ratio and small amount of copper oxides. The alloying Cu enhances the passivation ability and pitting corrosion resistance of the cold-rolled stainless steels.

**Keywords** Metastable austenitic stainless steel · Copper · Pitting corrosion · Passivation · Cold-rolling

## Introduction

The 200 series (Cr-Mn-Ni) stainless steels are traditionally used in construction, safety protection, domestic appliances, and other equipment that can withstand heavy loads. In recent years, with the demand for light-weight and higher security in the automotive industry, they have been gradually adopted in automotive space frames, fuel tanks, and other impact structures due to the superior strength and toughness [1–3]. There is an increasing interest to develop 200 series stainless steels.

The 200 series stainless steels belong to metastable austenitic stainless steel. They have the excellent properties of strength and ductility because of the martensitic transformation during plastic deformation. Strain-induced martensitic transformation involves the formation of  $\varepsilon$ - and  $\alpha'$ -martensite phases. According to Grässel et al. [4], a large amount of  $\alpha'$ -martensite will form during the deformation of high-Mn TRIP steel and enhance the elongation of the steel due to retardation

of local necking. Wu et al. [5] found that the strain-induced  $\varepsilon$ -martensite in super austenitic stainless steel increases at higher strain rates, which may significantly improve the ductility. Recent study also confirmed that high martensite volume fraction and ratio of  $\varepsilon$ - and  $\alpha'$ -martensite content are helpful to achieve higher tensile strength [6].

As an alloying element, Cu has great influence on the microstructure and properties of stainless steels [7–10]. The metastable austenite ( $\gamma$ ) in 200 series stainless steels can be transformed into  $\varepsilon$ - or  $\alpha'$ -martensite via the route  $\gamma \rightarrow \varepsilon \rightarrow \alpha'$  [4]. Cu addition increases the stacking fault energy of the stainless steels and contributes to the suppression of  $\varepsilon$ -martensite formation and strain hardening rate during deformation. Substituting Ni with Cu can achieve higher elongation and better formability and solve the problem of hot shortness damage during hot rolling [11]. In the literature, the Cu addition in austenitic stainless steels may favor the formation of protective passive films in acid solutions, but is still controversial for the pitting corrosion resistance [12, 13]. Hong et al. [14] believed that Cu in 304 stainless steel destroys the stability of the passive film. Ujiro et al. [15] found that the dissolved Cu from stainless steel may form metal deposits on the corrosion sites, which subsequently restrains the dissolution of the anodic areas.

To the best of our knowledge, there is limited report on the Cu addition into the cold-rolled 200 series austenitic stainless steels. In this work, three type 204 stainless steels with

✉ Moucheng Li  
mouchengli@shu.edu.cn

<sup>1</sup> Institute of Materials, School of Materials Science and Engineering, Shanghai University, 149 Yanchang Road, Shanghai 200072, China

<sup>2</sup> School of Metallurgical Engineering, Anhui University of Technology, Ma'an Shan 243032, China

<sup>3</sup> Shanghai Baosteel Research Institute, Shanghai 200431, China

different Cu contents and a cold rolling reduction of 15% were investigated on the microstructure evolution and corrosion resistance in chloride solution. The main purpose is to gain fundamental information for the fabrication and application of the low-cost and high-strength Cu-alloyed austenitic stainless steels.

## Experimental

The type 204 metastable austenitic stainless steel sheets were produced by Baosteel (Shanghai, China). The plates with the size of  $300 \times 100 \times 3$  mm were cut from the annealed sheets and unidirectionally cold-rolled by compression with a reduction about 15% at ambient temperature. Table 1 gives their chemical compositions. With the Cu addition from about 0.87 to 1.46%, the Cr and Ni contents decrease slightly in the steels. Test specimens were fabricated with a dimension of  $10 \times 10$  mm.

The phase was identified by X-ray diffractometry (XRD). The measurement was performed on a D/MAX2500V with a Cu tube at 40 kV 250 mA. Based on the principle that the total integrated intensity of all the diffraction peaks for each phase in the heterogeneous alloy is proportional to the volume fraction, the martensite volume fraction can be calculated with the following equation [16, 17].

$$V_i = \frac{(1/n) \sum_{j=1}^n (I_i^j / R_i^j)}{(1/n) \sum_{j=1}^n (I_\gamma^j / R_\gamma^j) + (1/n) \sum_{j=1}^n (I_{\alpha'}^j / R_{\alpha'}^j) + (1/n) \sum_{j=1}^n (I_\varepsilon^j / R_\varepsilon^j)} \quad (1)$$

where  $i$  means phase ( $i = \gamma, \alpha',$  and  $\varepsilon$ ),  $n$  is the number of peaks examined,  $I$  represents the integrated intensity of the  $i$  phase on the  $(hkl)$  plane.  $R$  is the material scattering factor given as

$$R_{hkl} = \left( \frac{1}{v^2} \right) \left[ |F|^2 P \left( \frac{1 + \cos^2 2\theta}{\sin^2 \theta \cos \theta} \right) \right] (e^{-2M}) \quad (2)$$

where  $v$  is the unit cell volume and can be calculated from the Bragg constant and the reflection angle.  $|F|^2$  and  $P$  are the structural factors and multiplicative factors of each crystal plane, respectively.  $e^{-2M}$  is a temperature factor and can be obtained by the Debye function.

**Table 1** Chemical compositions of the test materials (wt.%)

Steel	C	Si	Mn	Cr	Ni	Cu	N
SS0	0.06	0.35	9.25	15.51	1.50	0	0.138
SS1	0.06	0.28	9.43	14.74	1.30	0.87	0.143
SS2	0.07	0.32	9.19	14.67	1.24	1.46	0.146

To analyze the phase transition mechanism of austenite ( $\gamma$ ),  $\varepsilon$ -, and  $\alpha'$ -martensite in three stainless steels, field emission scanning electron microscopy (FE-SEM, Apollo 300) was used with electron beam backscatter diffraction (EBSD). EBSD samples were coarsely polished with an alumina suspension and subsequently electro-etched in an ethyl alcohol solution with 8% (by volume) perchloric acid at the operation voltage of 20.0 V.

The effect of Cu on the corrosion behavior of stainless steel was analyzed with a Princeton PAR 273A potentostat and a three-electrode electrochemical testing system. The specimen is used as the working electrode with an exposure area of  $1 \text{ cm}^2$ , a saturated calomel electrode (SCE) as the reference electrode, and a platinum electrode as the auxiliary electrode [18, 19]. The test solution was 3.5% (by mass) NaCl at  $25^\circ \text{C}$  according to the standard ASTM G61-2018. The specimen was ground to 1200# with water sandpaper and immersed in the solution for 2 h to reach the steady corrosion state. Electrochemical impedance spectroscopy (EIS) measurement was performed with an AC disturbance signal of 10 mV (rms) in the frequency from 99 kHz to 10 mHz. The impedance spectra were fitted by using ZSimpWin 3.21 software. The polarization curve was determined at a scan rate of  $0.333 \text{ mV s}^{-1}$  from the corrosion potential until the current density reached  $0.1 \text{ mA cm}^{-2}$ . The electrochemical tests were repeated three times with different specimens.

The corrosion morphology of the specimen surface after the polarization was observed by tungsten filament scanning electron microscope (SEM, HITACHI SU-1500). The passive films formed on specimen surfaces at 0 V vs SCE for 30 min in the test solution were characterized by X-ray photoelectron spectroscopy (XPS, ESCALAB 250Xi). Monochrome Al  $K_\alpha$  X-rays were used, operated at 150 eV pass energy, and calibrated using C1s with a binding energy of 284.6 eV. Data

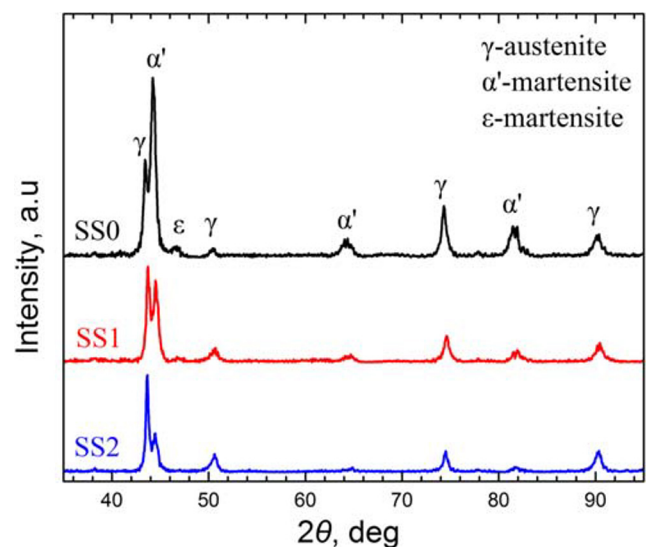
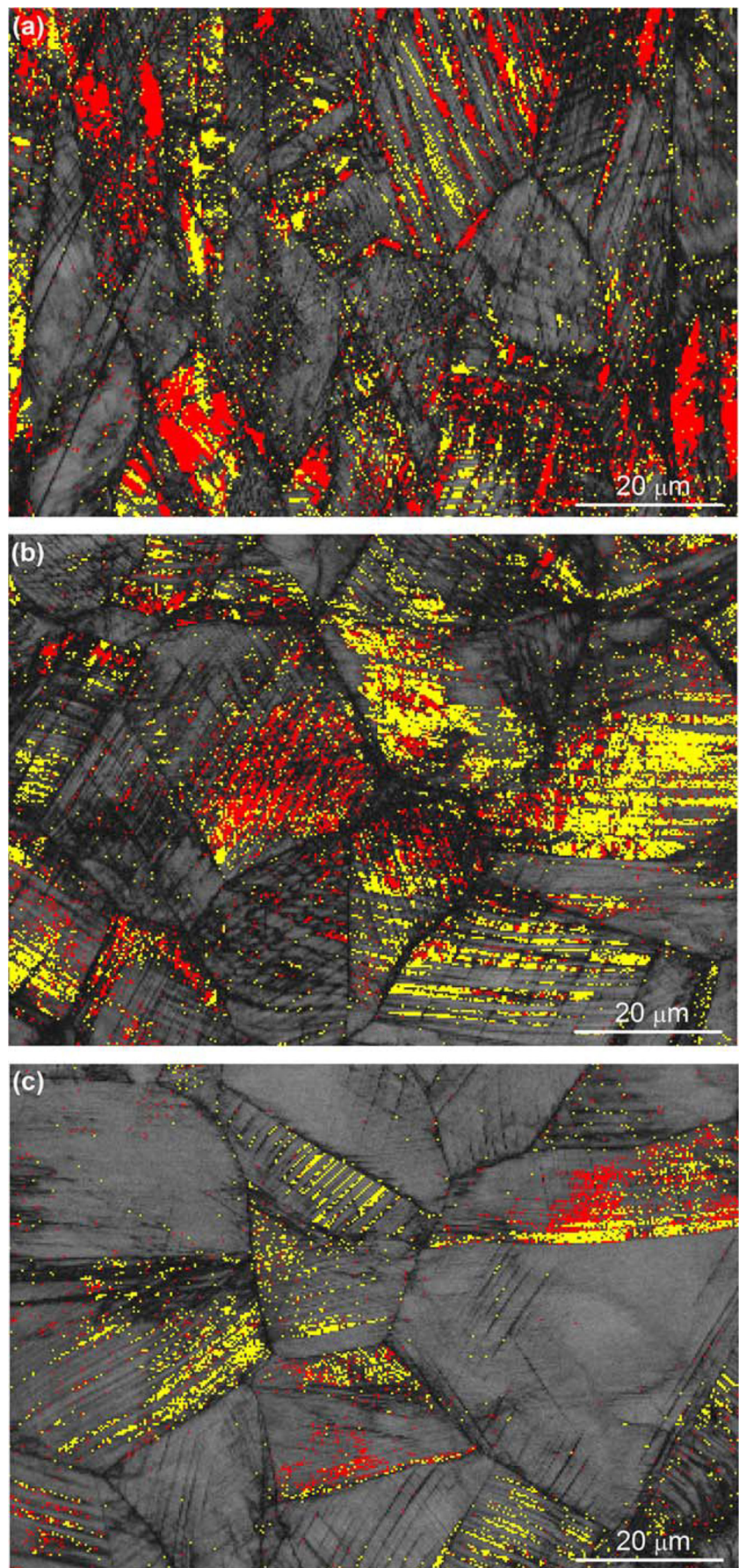


**Fig. 1** XRD patterns of the cold-rolled type 204 stainless steels with different Cu contents

**Fig. 2** EBSD observations for the cold-rolled type 204 austenitic stainless steels: **a** SS0, **b** SS1, and **c** SS2 (*red* for  $\alpha'$ -martensite, *yellow* for  $\varepsilon$ -martensite and gray for austenite)



processing was performed using Avantage software. The atomic ratio ( $r$ ) of Cr to Fe in the passivation film was calculated with the following equation [20]:

$$r_{\text{Cr/Fe}} = (I_{\text{Cr}}/S_{\text{Cr}})/(I_{\text{Fe}}/S_{\text{Fe}}) \quad (3)$$

where  $I$  is the measured peak area and  $S$  is the atomic sensitivity factor for Cr or Fe.

## Results

### Microstructure for cold-rolled metastable austenitic stainless steels

Figure 1 shows the X-ray diffraction patterns of the cold-rolled type 204 austenitic stainless steels with different Cu contents. With the Cu addition, the response peaks of  $\varepsilon$ - and  $\alpha'$ -martensite phases decrease noticeably, while the austenite ( $\gamma$ ) peaks increase gradually. The martensite volume contents were calculated using equations (1) and (2). The cold-rolled specimens have much higher  $\alpha'$ -martensite than  $\varepsilon$ -martensite. With the Cu addition of about 0.87 and 1.46%, the  $\alpha'$ -martensite content decreases markedly from about 50.3 to 37.1 and 17.7%, whereas the  $\varepsilon$ -martensite content decreases slightly from about 3.6 to 3.2 and 1.9%. At the same time, the austenite content increases from about 46.1 to 59.7 and 80.4%. These indicate that the alloying element Cu suppresses markedly the phase transformation during the cold-rolling processes and reduces greatly the volume content of deformation-induced martensite in type 204 metastable austenitic stainless steels.

Figure 2 gives the EBSD patterns for the type 204 austenitic stainless steels with 15% cold-rolling reduction. The  $\varepsilon$ ,  $\alpha'$ , and  $\gamma$  phases are shown in yellow, red, and gray, respectively. The austenitic structure is transformed partially into  $\varepsilon$ - and  $\alpha'$ -dislocation martensitic structures. The martensite content reduces significantly with increasing the Cu content. This is consistent with above XRD analysis. It is observed from the morphological positions in Fig. 2 that the  $\alpha'$ -martensites nucleate at the individual shear bands, intersections of shear bands, and some grain boundaries, whereas the  $\varepsilon$ -martensites mainly nucleate at the individual shear bands. Similar results were reported in the literature [6, 21–23].

### Electrochemical corrosion characteristics

Figure 3 shows the corrosion potential versus immersion time for the three stainless steels in 3.5% NaCl solution at 25 °C. The corrosion potentials increase slowly since the beginning of immersion and gradually reach the steady states after about 60 min. The stable corrosion potential values of SS0, SS1, and SS2 are about  $-148 \pm 8$ ,  $-120 \pm 5$ , and  $-109 \pm 3$  mV vs SCE, respectively, with a difference no more than 39 mV.

Obviously, the Cu addition less than 1.46% has insignificant influence on the corrosion potential of the cold-rolled type 204 austenitic stainless steels.

Figure 4 shows the impedance spectra for the three steels after 2 h of immersion in 3.5% NaCl solution at 25 °C. It is seen that all specimens exhibit the similar impedance characteristics. The Nyquist curves are composed of the single capacitive arcs in the testing frequency range, but the radius of the capacitive arc increases with the Cu content. This illustrates that the alloying element Cu can improve the corrosion resistance of the stainless steel. In the Bode curves, the time constants from the passive film and charge transfer process overlap together as a horizontal platform in the frequency range from about 20 to 0.1 Hz with almost invariable phase angle  $\theta$  values. The phase angles of the horizontal platform change slightly from about 81.3° to 82.5° with the Cu addition. These indicate that the protective films formed on the surfaces of all stainless steels in 3.5% NaCl solution [24].

Figure 5 gives the typical polarization curves for the three stainless steel specimens in 3.5% NaCl solution at 25 °C. With the Cu addition of about 0.87 and 1.46%, the pitting potential increases from about  $133 \pm 20$  to  $150 \pm 18$  and  $191 \pm 23$  mV vs SCE, whereas the passive current density at a given potential 0 V vs SCE decreases from about  $0.32 \pm 0.13$  to  $0.14 \pm 0.05$  and  $0.07 \pm 0.01$   $\mu\text{A cm}^{-2}$ . It is apparent that the alloying element Cu enhances the passive stability and the pitting corrosion resistance of type 204 austenitic stainless steel. This Cu-alloying effect was also observed on both ferritic and austenitic stainless steels with an addition of 3% Cu in 3 mol L<sup>-1</sup> NaCl solution at 60 °C [15] and martensitic stainless steels with 1.1–1.9% Cu in 0.5 mol L<sup>-1</sup> NaCl solution at 25 °C [25]. In addition, there are some current oscillations for the three steels in the passive regions in Fig. 5. They are frequently detected for austenitic stainless steels with high Mn contents and can be attributed to the generation of metastable pits [26, 27].

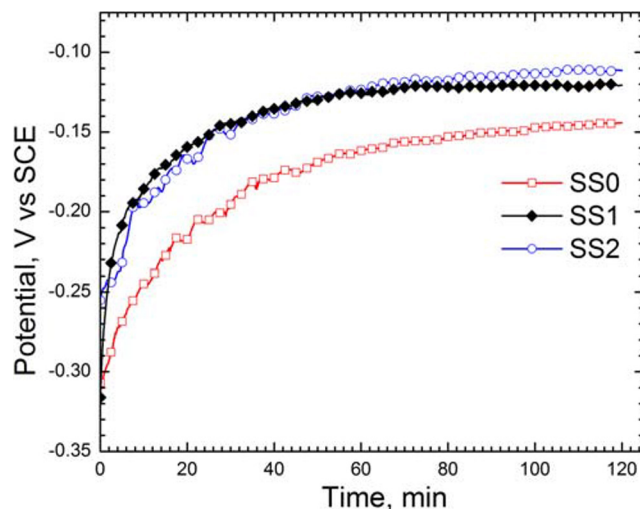


Fig. 3 Variation of corrosion potential with immersion time for the three steels in 3.5% NaCl solution at 25 °C

**Fig. 4** Impedance plots. **a** Nyquist and **b** Bode for the three steels in 3.5% NaCl solution at 25 °C (symbols: experimental data; lines: fitted values)

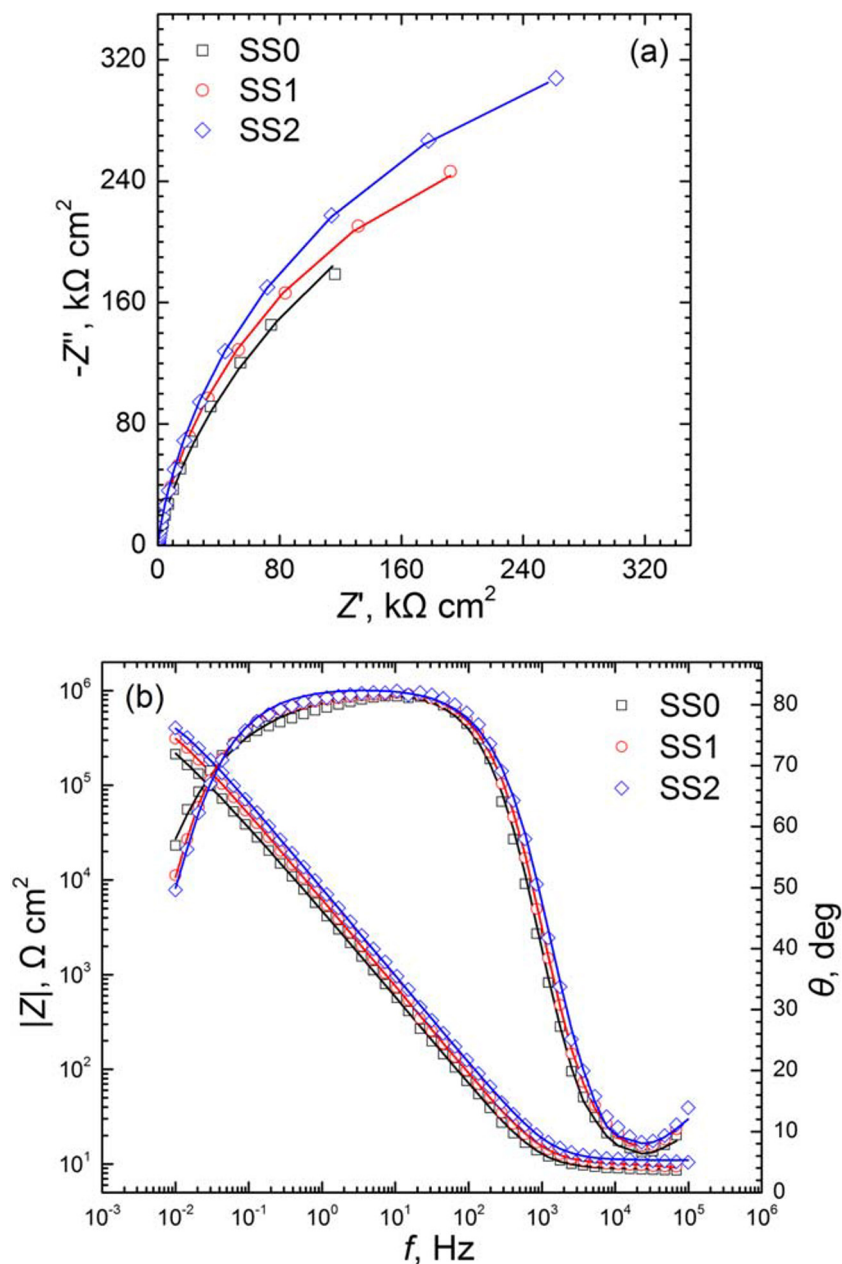
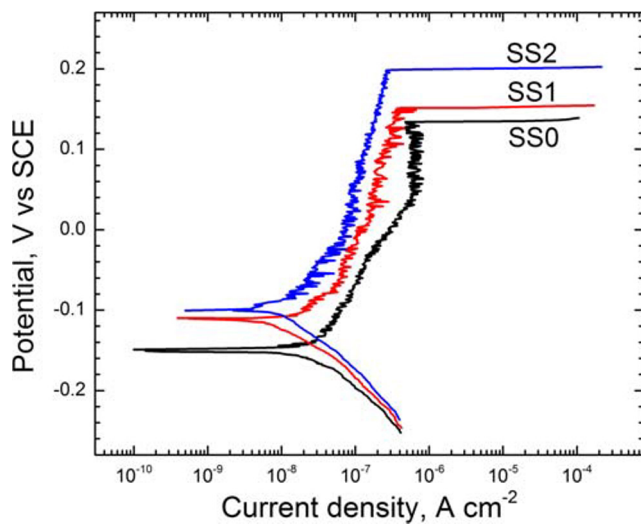


Figure 6 shows the morphologies for the maximum pits on the specimen surfaces after the polarization measurement in 3.5% NaCl solution at 25 °C. The maximum pits of the three steels have the similar size. In addition, all pits are open. The average pit numbers that appeared on the three parallel specimens of SS0, SS1, and SS2 are about 7, 3, and 3, respectively. This indicates that the alloying Cu inhibits the occurrence of stable pits on the cold-rolled type 204 austenitic stainless steels.

### XPS analysis of passive film

The XPS analysis was performed to provide chemical composition information on the passive films formed by the

potentiostatic polarization at 0 V vs SCE on the type 204 austenitic stainless steels in 3.5% NaCl solution. Figure 7 gives the XPS plots for the survey spectra and the detailed spectra of Cr 2p<sub>3/2</sub>, Fe 2p<sub>3/2</sub>, and Cu 2p<sub>3/2</sub> responses for different passive films on the three steels. In Fig. 7a, the survey spectra display the clear response peaks of Fe, Cr, O, N, and C and no (or very weak) signals of Ni and Mn for the passive films of all three steels. In addition, the passive films on SS1 and SS2 exhibit tiny response peaks of Cu. It is apparent that the passive films are mainly composed of Fe and Cr species. The three steels almost have similar N responses which may be assigned to the formation of mobile ions (e.g., NH<sub>4</sub><sup>+</sup>) in the passive films [28]. The disappearance of Ni and Mn usually



**Fig. 5** Potentiodynamic polarization curves of the three steels in 3.5% NaCl solution at 25 °C. Scan rate 0.333 mV s<sup>-1</sup>

results from their preferential dissolution in the presence of Cl<sup>-</sup> ions [29, 30]. The C responses can be attributed to the contamination in the environments [31].

The Cr 2p<sub>3/2</sub> spectra in Fig. 7b mainly show three peaks, i.e., metallic state Cr (574.4 ± 0.2 eV), Cr<sub>2</sub>O<sub>3</sub> (576.5 ± 0.2 eV), and Cr(OH)<sub>3</sub> (577.4 ± 0.2 eV). For the Cu-free steel SS0, Cr(OH)<sub>3</sub> peak is slightly higher than Cr<sub>2</sub>O<sub>3</sub> peak, while the intensity of Cr<sub>2</sub>O<sub>3</sub> peak becomes higher than that of Cr(OH)<sub>3</sub> as the Cu content increases from 0 to 0.87 to 1.46% for the steels SS1 and SS2.

The Fe 2p<sub>3/2</sub> response peaks in Fig. 7c can be fitted for the metallic Fe (707.2 ± 0.1 eV), FeO (709.4 ± 0.2 eV), Fe<sub>2</sub>O<sub>3</sub> (710.6 ± 0.2 eV), and FeOOH (711.6 ± 0.2 eV). Very weak Fe<sub>2</sub>O<sub>3</sub> peaks appear in the passive films on the three steel

surfaces. The relative intensity of metallic Fe peak gradually becomes weaker with the increase of Cu content in the stainless steels. The Cr/Fe ratios of passive films on the surfaces of SS0, SS1, and SS2 are about 1.10, 1.29, and 1.45, respectively. This indicates that the Cu addition slightly enlarges the Cr/Fe ratio value of the passive film. The alloying Cu will promote the relative enrichment of Cr<sup>3+</sup> species in comparison with the Fe<sup>2+</sup> and Fe<sup>3+</sup> species, which can be attributed to the preferential dissolution of Fe [30].

In Fig. 7d, the tiny response peaks of Cu 2p<sub>3/2</sub> appear at 932.5 ± 0.2 eV, which can be assigned to the metallic Cu and the oxides CuO and Cu<sub>2</sub>O. It is very hard to distinguish the peaks of Cu<sup>0</sup> and copper oxides because of the similar binding energies and very weak responses [24, 29]. The intensity of Cu 2p<sub>3/2</sub> peak becomes slightly stronger with the change of Cu content from 0.87 to 1.46%. It is clear that a small amount of copper oxides exists in the passive films.

## Discussion

According to the literature [6, 32, 33], the stainless steel deformation process can be resolved into two a/6<112> Shockley partial dislocations by a full dislocation. In the deformation process, partial dislocations sweep the alternate {111}γ plane to form the ε-martensite with the close-packed hexagonal structure, and metastable austenite with low stacking fault energy provides favorable conditions for ε-martensite nucleation [32]. The faults in different directions intersect with ε-martensite during the dynamic deformation process. These regions are areas of stress concentration that promote nucleation and growth of α'-martensite in high-density dislocation

**Fig. 6** The morphologies of the maximum pits formed on different specimen surfaces after the polarization measurement: a SS0, b SS1, and c SS2

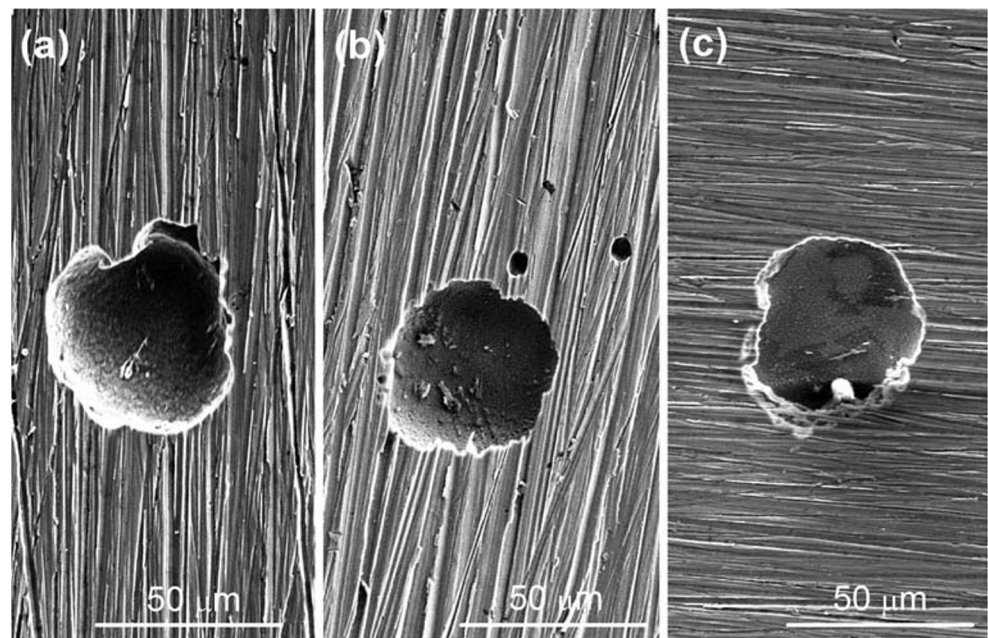
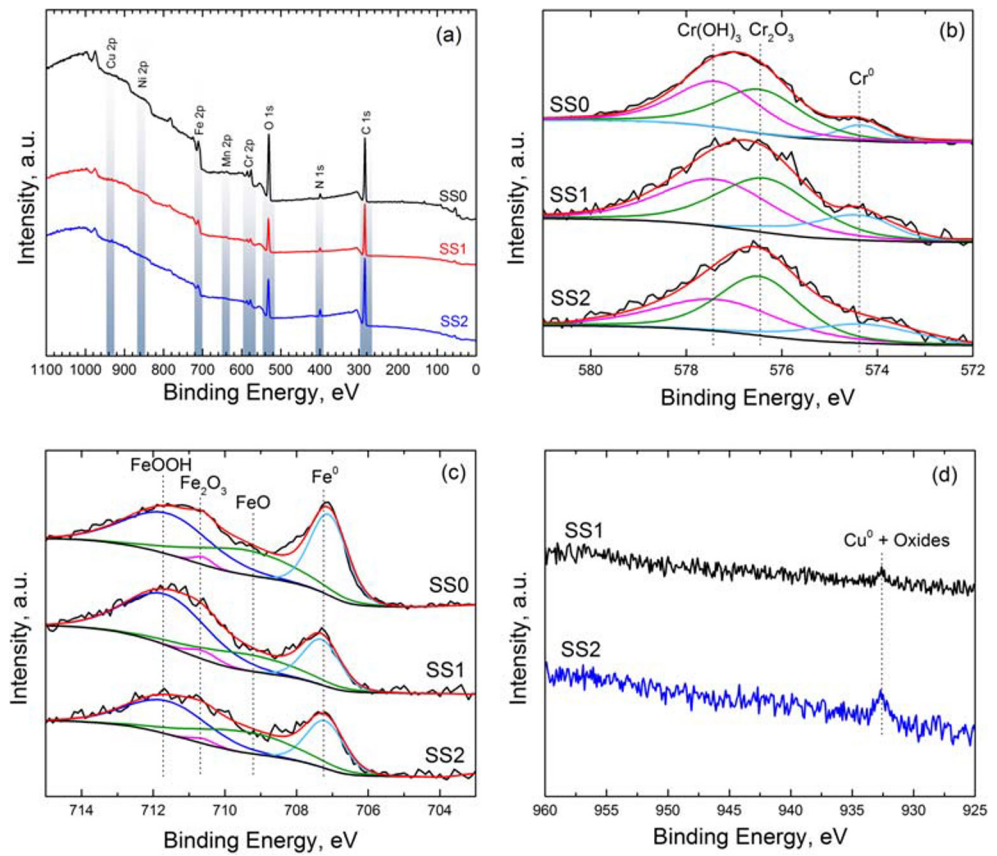


**Fig. 7** XPS plots for **a** the survey spectra and the detailed spectra, **b** Cr 2p<sub>3/2</sub>, **c** Fe 2p<sub>3/2</sub>, and **d** Cu 2p<sub>3/2</sub> for the passive films formed on the specimen surfaces after the potentiostatic polarization in 3.5% NaCl solution



zones [33]. The  $\epsilon$ -martensite is an intermediate phase of  $\gamma \rightarrow \alpha'$ -martensite transformation.

The alloying Cu plays an important role in the microstructures of the cold-rolled stainless steels, as shown in Figs. 1 and 2. The alloying Cu is an austenite-stabilizing element. It may increase the stacking fault energy of the stainless steels and reduce the sites of the  $\epsilon$ -martensite embryos [34, 35]. As a result, the martensite volume fraction decreases noticeably with increasing the Cu content from 0 to 0.87 to 1.46%. In addition, during the cold rolling process, a high density of dislocation substructures must form inside the lath martensite [36]. At the same time, the martensite phases will hinder the dislocation movement, leading to the dislocation increment in the austenite phases. Martensitic transformation brings not only high mechanical properties but also high density of

dislocation defects to the stainless steels. It can be assumed that the alloying Cu reduces the dislocation defects in the cold-rolled stainless steels through suppressing the martensitic transformation.

The impedance variation in Fig. 4 reflects the passivation and corrosion resistance of the specimens in 3.5% NaCl solution. The electrical equivalent circuit (EEC) [37, 38] in Fig. 8 was used to fit the EIS spectra, where  $R_s$  is the electrolyte resistance,  $R_f$  and  $C_f$  are the resistive and capacitive behavior of the passive film,  $R_t$  and  $C_{dl}$  represent the charge transfer resistance and the double layer capacitance, respectively, and are related to the oxidation-reduction processes occurring in the film [39]. In the fitting procedure, both  $C_f$  and  $C_{dl}$  were replaced with constant phase element (CPE) due to their non-ideal capacitive responses. Table 2 gives the average fitted values of three parallel specimens for the impedance parameters.  $R_p$  is the polarization resistance, which is theoretically equal to the sum of the resistances  $R_t$  and  $R_f$  [40].  $Y_0$  is the magnitude of admittance of CPE and  $\alpha$  is the exponential term. The relative errors from the fitting may reach about 15% for the parameters due to the incompletely defined semi-circles. As shown in Fig. 4, the simulated data show good coincidence with the experimental data in spite of the approximations made. It is seen that, with the Cu addition,  $Y_{0-f}$  and  $Y_{0-dl}$  gradually decrease from about  $(4.33 \pm 0.32) \times 10^{-5}$  to

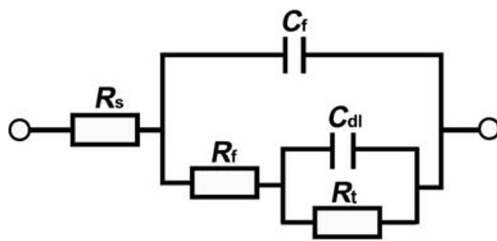


**Fig. 8** Equivalent circuit for the corrosion system of the specimens in 3.5% NaCl solution

**Table 2** Average fitted values with standard deviations from the impedance spectra of three parallel specimens in 3.5% NaCl solution

Steel	$R_s$ ( $\Omega \text{ cm}^2$ )	$Y_{0-f}$ ( $10^{-5} \text{ s}^\alpha \Omega \text{ cm}^{-2}$ )	$\alpha_f$	$Y_{0-dl}$ ( $10^{-5} \text{ s}^\alpha \Omega \text{ cm}^{-2}$ )	$\alpha_{dl}$	$R_p$ ( $10^5 \Omega \text{ cm}^2$ )
SS0	$9.8 \pm 0.9$	$4.33 \pm 0.32$	$0.88 \pm 0.03$	$3.18 \pm 0.29$	$0.86 \pm 0.03$	$6.20 \pm 0.61$
SS1	$10.3 \pm 0.6$	$3.56 \pm 0.22$	$0.91 \pm 0.02$	$2.69 \pm 0.23$	$0.92 \pm 0.02$	$6.71 \pm 0.48$
SS2	$10.6 \pm 0.3$	$2.79 \pm 0.14$	$0.90 \pm 0.01$	$2.03 \pm 0.12$	$0.91 \pm 0.03$	$8.02 \pm 0.44$

( $2.79 \pm 0.14$ )  $\times 10^{-5} \text{ s}^\alpha \Omega \text{ cm}^{-2}$  and ( $3.18 \pm 0.29$ )  $\times 10^{-5}$  to ( $2.03 \pm 0.12$ )  $\times 10^{-5} \text{ s}^\alpha \Omega \text{ cm}^{-2}$ , respectively, whereas  $R_p$  noticeably increases from about ( $6.20 \pm 0.61$ )  $\times 10^5$  to ( $8.02 \pm 0.44$ )  $\times 10^5 \Omega \text{ cm}^2$ . These indicate that the alloying Cu facilitates the formation of protective passive films and enhances the corrosion resistance of the cold-rolled Cr-Mn-Ni austenitic stainless steels in 3.5% NaCl solution.

Above results and analyses confirm that the alloying Cu is helpful to the passivation performance and pitting corrosion resistance of the cold-rolled type 204 stainless steels. In the literature [12–15], the influence of Cu on pitting potential depends on the potential range. The Cu addition shows a beneficial effect as the stable pitting corrosion takes place in the active potential range, but has a harmful effect in the noble potential range. It is apparent from Fig. 5 that the pitting potential values are in the active potential range. In addition, the three steels have a cold-rolling reduction of about 15%, which is different to the literature [12, 15]. The Cu action in this work may be mainly related to the following features. First, the deformation-induced  $\alpha'$ -martensite and defects (e.g., dislocations) may act as the active sites of pitting corrosion [41–43]. The dislocations facilitate the formation of oxygen vacancies and will reduce the compactness of the passive films [44]. It is inferred from Figs. 1 and 2 that the number of active sites on the steel surface must decrease with increasing the Cu content. Second, the noble alloying element Cu in the steels SS1 and SS2 may decrease the anodic dissolution of steel matrixes, especially the alloying element Cr, by blocking the active centers of crystal lattice structure [45]. This is presented as the preferential dissolution of Fe and the enrichment of Cr in the passive films [30, 46]. As obtained by above XPS analyses, the Cu addition will result in the Cr/Fe ratio enlargement of the passive film. It is well known that the higher Cr-species (i.e., oxide and hydroxide) content facilitates the formation of more stable passive film with the fewer defects on stainless steel [46, 47]. Third, a small amount of copper oxides may form in the passive films of SS1 and SS2 through the following reactions [48]:



According to the literature [29, 48–51], the copper oxides  $\text{Cu}_2\text{O}$  and  $\text{CuO}$  are stable and hence beneficial to improve the

passivation behavior of stainless steel. Clearly, these are mainly responsible for the lower values of passive current density,  $Y_{0-f}$  and  $Y_{0-dl}$  and the higher values of pitting potential and  $R_p$  with the increase of Cu content in the stainless steels.

## Conclusions

The effect of alloying element Cu (0.87 and 1.46%) on the microstructure and electrochemical corrosion behavior in 3.5% NaCl solution were investigated for the type 204 metastable austenitic stainless steels cold-rolled with a reduction of 15%. The main conclusions are drawn as follows:

- (1) The alloying Cu in the type 204 austenitic stainless steel suppresses the martensite phase transformation during the cold-rolling process. With the increase of Cu content from 0 to 1.46%, the volume fraction of  $\alpha'$ -martensite changes markedly from about 50.3 to 17.7%, whereas the  $\varepsilon$ -martensite fraction decreases slightly from about 3.6 to 1.9%.
- (2) With the Cu addition, the cold-rolled type 204 austenitic stainless steels show lower passive current density values and higher pitting potential and polarization resistance values in 3.5% NaCl solution. These mainly result from the alloying Cu actions, i.e., the reduction of martensite fractions and dislocation defects in the steels and the formation of passive films with higher Cr/Fe ratio and small amount of copper oxides.

**Funding information** Financial support was provided by National Natural Science Foundation of China (Grant Nos. U1960103 and U1660205).

## References

1. Kim YH, Kim KY, Lee YD (2004) Nitrogen-alloyed, metastable austenitic stainless steel for automotive structural applications. *Mater Manuf Process* 19(1):51–59
2. Jacques P, Fumémont Q, Mertens A, Delannay F (2001) On the sources of work hardening in multiphase steels assisted by transformation-induced plasticity. *Philos Mag A* 81(7):1789–1812
3. Joseph MJ, Jabbar MA (2019) Effect of aging process on the microstructure, corrosion resistance and mechanical properties of stainless steel AISI 204. *Case Stud Constr Mater* 11:e00253



4. Grässel O, Frommeyer G (1998) Effect of martensitic phase transformation and deformation twinning on mechanical properties of Fe–Mn–Si–Al steels. *Mater Sci Technol* 14(12):1213–1217
5. Wu CC, Wang SH, Chen CY, Yang JR, Chiu PK, Fang J (2007) Inverse effect of strain rate on mechanical behavior and phase transformation of superaustenitic stainless steel. *Scripta Mater* 56(8):717–720
6. Zhang YC, Li MC, Bi HY, Gu JQ, Chen DX, Chang E, Zhang W (2018) Martensite transformation behavior and mechanical properties of cold rolled metastable Cr–Mn–Ni–N austenitic stainless steels. *Mater Sci Eng A* 724:411–420
7. Charles J (2007) The new 200-series: an alternative answer to Ni surcharge? Risks or opportunities? *Rev Met Paris* 104(6):308–317
8. Tavares SM, Pardal JM, Silva MJGD, Abreu HFG, Silva MRD (2009) Deformation induced martensitic transformation in a 201 modified austenitic stainless steel. *Mater Charact* 60(8):907–911
9. Xi T, Shahzad M, Xu D, Zhao JL, Yang CG, Qi M, Yang K (2016) Copper precipitation behavior and mechanical properties of Cu-bearing 316L austenitic stainless steel: a comprehensive cross-correlation study. *Mater Sci Eng A* 675:243–252
10. Phaniraj MP, Shin YM, Lee J, Goo NH, Kim DL, Suh JY, Jung WS, Shim JH, Choi IS (2015) Development of high strength hot rolled low carbon copper-bearing steel containing nanometer sized carbides. *Mater Sci Eng A* 633:1–8
11. Gonzalez BM, Castro CSB, Buono VTL, Vilela JMC, Andrade MS, Moraes JMD, Mantel MJ (2003) The influence of copper addition on the formability of AISI 304 stainless steel. *Mater Sci Eng A* 343(1–2):51–56
12. Pardo A, Merino MC, Carboneras M, Coy AE, Arrabal R (2007) Pitting corrosion behaviour of austenitic stainless steels with Cu and Sn additions. *Corros Sci* 49(2):510–525
13. Sourisseau T, Chauveau E, Baroux B (2005) Mechanism of copper action on pitting phenomena observed on stainless steels in chloride media. *Corros Sci* 47(5):1097–1117
14. Hong IT, Koo CH (2005) Antibacterial properties, corrosion resistance and mechanical properties of Cu-modified SUS 304 stainless steel. *Mater Sci Eng A* 393(1–2):213–222
15. Ujiro T, Satoh S, Staehle RW, Smyrl WH (2001) Effect of alloying Cu on the corrosion resistance of stainless steels in chloride media. *Corros Sci* 43(11):2185–2200
16. De AK, Murdock DC, Mataya MC, Speer JG, Matlock DK (2004) Quantitative measurement of deformation-induced martensite in 304 stainless steel by X-ray diffraction. *Scripta Mater* 50(12):1445–1449
17. Zhang YC, Li MC, Bi HY, Chen DX, Gu JQ, Chang E (2019) Mechanical properties of cold-rolled metastable Cr–Mn–Ni–N austenitic stainless steel at low ambient temperature. *Mater Sci Eng A* 759:224–233
18. Elsener B, Addari D, Coray S, Rossi A (2011) Nickel-free manganese bearing stainless steel in alkaline media-electrochemistry and surface chemistry. *Electrochim Acta* 56(12):4489–4497
19. Luo H, Dong CF, Xiao K, Li XG (2011) Characterization of passive film on 2205 duplex stainless steel in sodium thiosulphate solution. *Appl Surf Sci* 258(1):631–639
20. Wagner CD, Riggs WN, Davies LE, Moulder JF, Muilenberg GE (1978) Handbook of X-ray photoelectron spectroscopy. Perkin Elmer Co., Eden Prairie
21. Liu JB, Chen CC, Feng Q, Fang XY, Wang HT, Liu F, Lu J (2017) Dislocation activities at the martensite phase transformation interface in metastable austenitic stainless steel: an in-situ TEM study. *Mater Sci Eng A* 703:236–243
22. Das A, Sivaprasad S, Ghosh M, Chakraborti PC, Tarafder S (2008) Morphologies and characteristics of deformation induced martensite during tensile deformation of 304LN stainless steel. *Mater Sci Eng A* 486(1–2):283–286
23. Lee H, Jo MC, Sohn SS, Zargarani A, Ryu JH, Kim NJ, Lee S (2018) Novel medium-Mn (austenite + martensite) duplex hot-rolled steel achieving 1.6 GPa strength with 20% ductility by Mn-segregation-induced TRIP mechanism. *Acta Mater* 147:247–260
24. Luo H, Li XG, Dong CF, Xiao K (2013) The influence of Cu on the electrochemical behaviour of 304 stainless steel in 0.1M H<sub>3</sub>PO<sub>4</sub> solution. *Surf Interface Anal* 45(4):793–799
25. Geng HM, Wu XC, Wang HB, Min YA (2008) Effects of copper content on the machinability and corrosion resistance of martensitic stainless steel. *J Mater Sci* 43(1):83–87
26. Pardo A, Merino MC, Coy AE, Viejo F, Arrabal R, Matykina E (2008) Pitting corrosion behaviour of austenitic stainless steels-combining effects of Mn and Mo additions. *Corros Sci* 50(6):1796–1806
27. Yang Y, Zeng HT, Xin SS, Hou XL, Li MC (2020) Electrochemical corrosion behavior of 2205 duplex stainless steel in hot concentrated seawater under vacuum conditions. *Corros Sci* 165:108383
28. Olsson COA (1995) The influence of nitrogen and molybdenum on passive films formed on the austenoferritic stainless steel 2205 studied by AES and XPS. *Corros Sci* 37(3):467–479
29. Raov VS, Singhal LK (2009) Electrochemical and surface analytical approach to passive film on 200 series stainless steels formed in sulfuric acid. *ISIJ Int* 49:1902–1906
30. Kocijan A, Donik C, Jenko M (2007) Electrochemical and XPS studies of the passive film formed on stainless steels in borate buffer and chloride solutions. *Corros Sci* 49(5):2083–2098
31. Wang C, Jiang F, Wang FH (2004) The characterization and corrosion resistance of cerium chemical conversion coatings for 304 stainless steel. *Corros Sci* 46(1):75–89
32. Olson GB, Cohen M (1972) A mechanism for the strain-induced nucleation of martensitic transformations. *J Less-Common Met* 28(1):107–118
33. Murr LE, Staudhammer KP, Hecker SS (1982) Effects of strain state and strain rate on deformation-induced transformation in 304 stainless steel: part II. Microstructural study. *Metall Mater Trans A* 13(4):627–635
34. Dumay A, Chateau JP, Allain S, Migot S, Bouaziz O (2008) Influence of addition elements on the stacking-fault energy and mechanical properties of an austenitic Fe–Mn–C steel. *Mater Sci Eng A* 483–484:184–187
35. Frommeyer G, Brück U (2006) Microstructures and mechanical properties of high-strength Fe–Mn–Al–C light-weight TRIPLEX steels. *Steel Res Int* 77(9–10):627–633
36. Natutani T (1989) Effect of deformation-induced martensitic transformation on the plastic behavior of metastable austenitic stainless steel. *Mater Trans* 30(1):33–45
37. Li MC, Wang SD, Ma RY, Han PH, Bi HY (2012) Effect of cyclic oxidation on electrochemical corrosion of type 409 stainless steel in simulated muffler condensates. *J Solid State Electrochem* 16(9):3059–3067
38. Xin SS, Li MC (2014) Electrochemical corrosion characteristics of type 316L stainless steel in hot concentrated seawater. *Corros Sci* 81:96–101
39. Freire L, Carneim MJ, Ferreira MGS, Montemor MF (2010) The passive behaviour of AISI 316 in alkaline media and the effect of pH: a combined electrochemical and analytical study. *Electrochim Acta* 55(21):6174–6181
40. Kocijan A, Merl DK, Jenko M (2011) The corrosion behaviour of austenitic and duplex stainless steels in artificial saliva with the addition of fluoride. *Corros Sci* 53(2):776–783
41. Mandel M, Böhme F, Hauser M, Wendler M, Tuchscheerer F, Krüger L (2016) The influence of plastic deformation on the corrosion behavior of a cast high-alloy CrMnNi TRIP steel. *Steel Res Int* 87(8):1105–1110

42. Mudali UK, Shankar P, Ningshen S, Dayal RK, Khatak HS, Raj B (2002) On the pitting corrosion resistance of nitrogen alloyed cold worked austenitic stainless steels. *Corros Sci* 44(10):2183–2198
43. Zhang YC, Li MC, Bi HY (2019) The mechanism of pitting initiation and propagation at deformation bands intersection of cold-rolled metastable stainless steel in acidic ferric chloride solution. *J Mater Sci* 54(24):14914–14925
44. Lv JL, Guo WL, Liang TX (2016) The effect of pre-deformation on corrosion resistance of the passive film formed on 2205 duplex stainless steel. *J Alloys Compd* 686(25):176–183
45. Hermas AA, Ogura K, Adachi T (1995) Accumulation of copper layer on a surface in the anodic polarization of stainless steel containing Cu at different temperatures. *Electrochim Acta* 40(7):837–844
46. Oh KN, Toor IH, Ahn SH, Kwon HS (2013) Effects of Cu on the passive film stability of Fe-20Cr-xCu ( $x = 0, 2, 4$  wt.%) alloys in  $H_2SO_4$  solution. *Electrochim Acta* 88:170–176
47. Asami K, Hashimoto K, Shimodaira S (1977) XPS determination of compositions of alloy surfaces and surface oxides on mechanically polished iron-chromium alloys. *Corros Sci* 17(9):713–723
48. Babic R, Metikos-Hukovic M, Jukic A (2001) A study of copper passivity by electrochemical impedance spectroscopy. *J Electrochem Soc* 148(4):B146–B151
49. Adeloju SB, Duan YY (1994) Corrosion resistance of  $Cu_2O$  and  $CuO$  on copper surfaces in aqueous media. *Br Corros J* 29(4):309–314
50. Pardo A, Merino MC, Carboneras M, Viejo F, Arrabal R, Muñoz J (2006) Influence of Cu and Sn content in the corrosion of AISI 304 and 316 stainless steels in  $H_2SO_4$ . *Corros Sci* 48(5):1075–1092
51. Kim ST, Park YS (2007) Effect of copper addition on corrosion behavior of high-performance austenitic stainless steel in highly concentrated sulfuric acid solution-part 1. *Corrosion* 63(2):114–126

**Publisher's note** Springer Nature remains neutral with regard to jurisdictional claims in published maps and institutional affiliations.